Mineral. Deposita 31, 432–438 (1996)

MINERALIUM DEPOSITA

Mineralogical and geochemical characteristics of two bauxitic profiles, Fria, Guinea Republic

B. Boulangé[1], G. Bouzat[2], M. Pouliquen[3]

[1]ORSTOM, UM GECO, CEREGE, Université Aix Marseille III, Europôle Méditerranéen de l'Arbois, BP 80, Aix en Provence Cedex 4
[2]Pechiney, BP 54, 13541 Gardanne, France
[3]Société des Feldspaths du Morvan, 71400 Autun, France

Received: 1 November 1993/Accepted: 14 December 1995

Abstract. Bauxite deposits of the Fria district, Guinea, have been exploited since 1960. These lateritic bauxites, located on the upper parts of plateaus, result from weathering of paleozoic schists. The ores are composed of gibbsite associated with pyrophyllite, Al-substituted gœthite, and kaolinite. Pyrophyllite and Al-substituted gœthite may contain up to 9% of the total Al_2O_3 content of the bauxite; this cannot be recovered through the Bayer process because these phases are insoluble in the leaching solutions. Kaolinite is soluble under Bayer leaching but this dissolution induces precipitation of sodium aluminosilicates, which apart from loss of further alumina results in decreasing efficiency of the process through scale formation. Detailed knowledge of the distribution of the different ore types and their mineralogical composition is necessary for efficient processing.

The Fria bauxite deposit is located in western part of the Guinea Republic, between N10°20′–10°30′ and W13°30′–13°40′. Within the general area of bauxitization there are about 20 small ore deposits, each containing between 2 and 20 Mt. Prospecting commenced in 1955 and mining in 1960. The deposit lies at the junction of the Konkouré and Badi rivers, both of which deeply incise surrounding plateaus (200–260 m) and hills (280–320 m) (Fig. 1).

The Fria area has a humid tropical climate. The rainy season occurs between May and November, with an average annual precipitation of 3600 mm. Monthly average temperatures vary from 24 °C to 28 °C. On plateaus, weathering mantle zones covered with grasses alternate with fractured mantle zones with forest cover. Steep slopes are often characterized by dense vegetation but, as a result of human activity, valleys contain only traces of their previous forest cover.

The Fria bauxite deposits formed on the Paleozoic cover of the West African Craton, which was uplifted during the Tertiary along the Guinean axis (Bessolles 1977; Boulangé and Millot 1988). Deposits are mostly developed on Gothlandian schists which are enclosed by two thick Ordovician and Devonian sandstone series (Villeneuve 1984). These schists outcrop over a SE-NW-trending, 25 km wide belt in the north of the Fria-Kimbo district, and are strongly fractured by NE-trending strike-slip faults. The lower part of the series consists of blue to grey-blue, finely bedded aluminous schists overlain by a shaley sandstone. The upper part of the series is composed of alternating sandstones and sericite-schists. Dolerite intrudes this series as sills up to 10 m thick and, less frequently, as dykes.

This Paleozoic series is sub-horizontal and has been intensely fractured during Hercynian earth movements. Relative displacement of segments has resulted in a variety of rocks being exposed to lateritic weathering at outcrop. These weathered rocks now occur on SW–NE-striking plateaus separated by structural saddles or lateritic crusts. The bauxite ores are found on the plateaus. On the Fria tableland, bauxites also extend as gently sloping lobes into the main valley. Lithological variability of bedrock, geomorphological variations, presence or absence of vegetation, and differences in intensity of faulting and fracturing, all contribute to the diversity of the weathering profiles. The aim of the present study was to define mineral parageneses in two typical bauxite profiles, in the hope that these could explain compositional variations, mainly in silica content, which influence quality.

Weathering patterns

Observations conducted during mining and on drill cores have indicated a consistency within the lateritization profiles, which can reach thicknesses of 25–30 m. Three macroscopic units in the weathering cover can be distinguished which from top to bottom comprise (a) a friable, sandy-clay layer, (b) a bauxitic crust, (c) a weathered rock.

The *friable sandy-clay surficial layer*, yellowish brown to black in colour, is ubiquitous in the Fria district, but its thickness is influenced by the type of vegetation cover. On profiles where the vegetation is only herbaceous, it is very thin (0–20 cm) and contains

Correspondence to: B. Boulangé

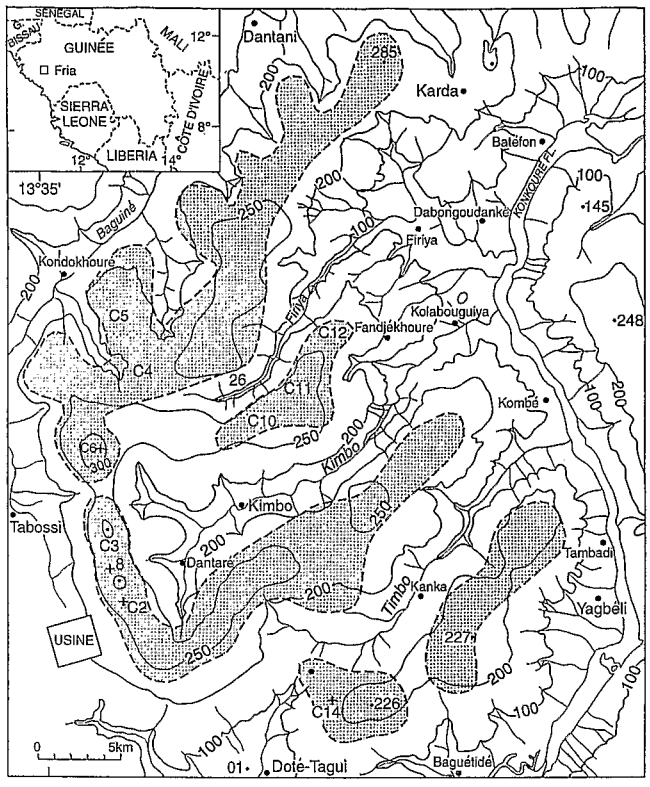

Fig. 1. Map of bauxite ores location (*stippled area*) of Fria, Guinea

blocks and nodules of the underlying bauxitic crust, the nodules being rounded and covered by a black patina. Under forest, this layer can exceed one metre, the upper part of which is rich in black humic material. With depth it becomes lighter in colour; nodules of bauxitic crust are still abundant, but these are angular and lack the patina. The matrix of this layer is composed of kaolinite and small grains of quartz.

The *bauxitic crust* forms the ore. Apart from on steep valley sides and the lower parts of slopes, this crust is ubiquitous. Its thickness varies from one to six metres. This dense and massive hardpan shows different physical characteristics depending on the topography. On hills, the crust is fragmented forming large slabs or boulders up to several meters across, separated by distinct fractures typically penetrated by tree roots. This type of bauxite shows three facies: platy, porous and vesicular, and composite. On structural saddles, the crust is massive, dense and very ferruginous, and brown to deep reddish-brown in colour. It is either compact, breaking with a clean fracture, or porous and vesicular. Light-coloured slaty residual rock fragment may be included in the matrix. On pediments and shallow slopes, the crust is fragmented and heterogeneous, consisting of irregular hardpan fragments and nodules within an argillo-ferruginous matrix. With increase in slope angle, evidence of mechanical reworking becomes evident with the appearance of conglomeratic crusts: nodules and boulder blocks from upper levels are mixed with pebbles originating from old alluvial terraces.

The transition zone from crust to *weathered rock* is progressive, irregular and usually 2–3 m thick. The crust is fragmented into boulders and nodules which decrease in size with depth. These fragments are embedded in a red, clayey and friable matrix, the amount of which increases with depth. The weathered layer can be divided into an upper layer or "alloterite" in which the parent-rock texture has disappeared and a lower layer or "isalterite" where this is still visible. The predominant *parent rocks* identified at the base of profiles are schistose sandstones, with only rare occurrences of dolerites.

Materials and methods

Two series of samples were selected for study (Fig. 1).

Samples 1–6 collected in quarry C14, located on footslope of a pediment, and sample 8 from quarry C2.

1C14 porous and vesicular bauxite
2C14 platy ferruginous bauxite
3C14 porous ferruginous bauxite
4C14 porous bauxite
5C14 bauxite-alloterite transition (split into two subsamples: 5-bauxite, 5m-matrix)
6C14 alloterite: red clay (split into two subsamples: 6a-matrix, 6b-nodules)
8C2 isalterite: weathered blue schist

Samples 12–17, collected in quarry C6, located on a hilltop,

12C6 platy bauxite (split into three subsamples: 12a, 12b, 12c)
13C6 porous and vesicular bauxite
14C6 bauxite-alloterite transition
15C6 tubular bauxite (split into two subsamples: 15a, 15b)
16C6 alloterite: red-brown clay
17C6 isalterite: weathered blue schist

A sample of fresh schist (26) was also collected from the Firiya river bank, as this was considered typical of predominant rock in the area.

Sample textures were examined using both optical and scanning electron microscopy. Mineralogical examination was conducted by microprobe and by X-ray diffractometry (Mondielli 1991). Chemical analyses were carried out by inductively-coupled plasma-optical emission spectrometry (ICP-OES).

Bauxitic facies petrography

The relatively low sample density used has not allowed definitive relationships between facies to be determined. However, when chemical data from Table 1 are plotted on a SiO_2-Al_2O_3-Fe_2O_3 diagram (Fig. 2), three fields can be distinguished corresponding to bauxites, ferruginous bauxites and argillo-ferruginous bauxites. Mineralogical, chemical and textural features of samples from these three groups are described next.

Bauxites

These are high in alumina (56–60% Al_2O_3), and have Fe_2O_3 contents ranging from 1–8% and SiO_2 contents ranging from 1–12%. Within this group, bauxites *sensu stricto* and pyrophyllite-rich bauxites may be distinguished.

The only sample bauxites *s.s.* (4C14) is porous, yellow in colour, and has a platy texture. Plates, which exhibit the original schistose texture, are regularly bedded but are strongly jointed perpendicular to bedding planes. The plates, on average 10 cm thick, occur within a matrix rich in iron and alumina. Overall, such bauxites are characterized by alternating lighter and darker beds, the former consisting mainly of well-crystallized gibbsite. The darker beds (30–50 cm thick) contain gibbsite, gœthite and small amounts of hematite. Later gibbsite veins cut across both lighter and darker beds. The average mineralogical composition of this sample is 76% gibbsite, 16% aluminous gœthite, 4% kaolinite, 3% anatase and 0.5% hematite. The aluminous gœthite shows about 20 mol% Al for Fe substitution, which represents about 6% of the total Al_2O_3 content of the sample.

Table 1. Chemical analyses of major elements (wt%), trace elements and REE (ppm) from Fria bauxitic profiles, Guinea

	Profile C.14								C2	Profile C6									
	1	2	3	4	5	5m	6a	6b	8	12a	12b	12c	13	14	15a	15b	16	17	26
Density	2.13	2.69	2.23	2.09	2.69	2.69	1.74	1.74	1.87	2.32	2.32	2.32	1.91	1.76	2.29	2.13	1.47	1.80	2.60
SiO_2	1.08	1.42	1.15	1.55	1.29	7.45	19.93	1.97	15.43	6.52	5.46	10.04	4.35	12.53	12.02	8.26	27.73	34.91	68.99
Al_2O_3	42.99	41.10	38.46	56.43	24.92	31.70	36.65	46.19	43.61	59.97	60.68	58.57	40.15	37.94	59.85	56.58	29.12	39.96	16.75
Fe_2O_3	27.04	32.92	35.57	8.21	53.48	39.47	21.20	23.39	15.62	1.89	2.84	2.25	29.64	27.97	0.93	7.06	24.85	6.42	5.99
TiO_2	3.37	2.61	3.56	2.99	1.17	1.96	2.71	2.28	2.60	1.44	1.44	2.94	2.33	2.12	1.05	0.82	2.13	1.91	1.44
MnO	0.09	0.02	0.09	0.02	0.01	0.02	0.02	0.02	0.01	0.01	0.01	0.01	0.11	0.11	0.01	0.03	0.11	0.01	0.04
MgO	0.02	0.03	0.06	0.02	0.05	0.17	0.26	0.03	0.05	0.01	0.01	0.01	0.03	0.06	0.02	0.01	0.09	0.38	0.57
CaO	0.02	0.02	0.06	0.06	0.10	0.08	0.07	0.05	0.01	0.02	0.02	0.04	0.02	0.04	0.04	0.01	0.03	0.06	0.40
Na_2O	0.06	0.04	0.01	0.08	0.02	0.12	0.26	0.04	0.09	0.13	0.11	0.15	0.01	0.01	0.54	0.11	0.01	0.63	0.64
K_2O	0.01	0.02	0.01	0.02	0.02	0.12	0.31	0.03	0.02	0.02	0.02	0.01	0.02	0.02	0.20	0.03	0.01	2.89	2.79
H_2O^+	23.70	21.80	21.22	28.15	18.02	17.77	17.00	24.22	20.57	27.70	27.82	25.58	21.35	18.37	25.07	27.05	13.35	13.22	3.85
Total	98.38	99.98	100.19	97.53	99.08	98.86	98.41	98.22	98.01	97.71	98.41	99.60	98.01	99.17	99.73	99.96	97.43	100.39	101.46
Rb	3	2	3	1	3	5	19	3	2	1	2	2	2	2	11	2	1	106	54
Sr	1	2	12	1	9	27	36	18	1	1	1	1	2	2	24	1	1	86	95
Cr	414	404	872	584	693	480	351	766	315	165	86	153	196	318	152	631	364	185	109
Ni	16	15	69	12	10	9	14	10	2	4	6	4	36	54	16	29	84	17	11
V	473	279	524	245	476	404	336	331	309	145	126	151	151	469	439	130	143	472	207
Zn	85	48	59	44	56	29	27	32	11	3	3	5	103	98	2	52	99	8	62
Y	22	42	16	44	31	31	50	33	49	23	77	46	21	14	115	11	12	24	78
Zr	499	1040	450	965	731	711	1114	740	496	360	535	485	336	323	257	269	260	250	577
Nb	41	44	41	56	40	46	60	43	45	27	28	45	26	28	46	26	27	25	29
La	13.60	14.60	11.60	34.80	14.30	23.60	24.80	32.80	16.10	28.50	5.59	102.00	5.05	11.60	44.20	3.24	7.78	11.00	60.20
Ce	26.40	23.60	28.30	49.50	21.30	44.70	48.00	45.80	25.10	61.00	14.40	214.00	52.50	22.30	91.00	6.92	21.50	11.60	129.00
Nd	8.96	9.70	7.18	22.30	8.09	11.70	14.65	22.10	6.08	21.60	4.84	82.00	3.60	7.82	32.60	2.17	7.17	5.56	50.10
Sm	1.68	1.78	1.36	3.64	1.51	2.71	2.63	4.47	1.41	4.16	0.83	17.10	0.88	1.87	5.95	0.50	1.92	1.03	10.30
Eu	0.41	0.46	0.28	0.75	0.30	0.42	0.56	1.02	0.84	0.83	0.22	2.73	0.24	0.51	0.81	0.11	0.55	0.47	2.07
Gd	1.71	1.76	1.27	2.45	1.33	1.84	2.41	3.01	2.06	2.38	0.77	11.40	0.70	1.65	3.36	0.58	2.16	1.26	7.97
Dy	2.44	2.50	1.79	3.00	1.40	2.28	3.36	3.01	3.71	1.89	0.98	7.97	1.35	2.33	2.69	0.90	2.92	2.07	7.87
Yb	2.30	2.57	1.83	2.70	1.29	2.15	2.92	2.10	3.18	1.35	1.22	3.21	1.32	1.98	1.32	0.91	2.05	1.76	4.17
Lu	0.45	0.48	0.36	0.48	0.30	1.65	0.51	0.39	0.58	0.27	0.24	0.57	0.14	0.18	0.32	0.21	0.22	0.16	0.70

The pyrophyllite-rich bauxites exhibit a granular texture with platy or tubular jointing. Those with platy jointing (sample 12C6) show alternating dense grey beds and porous light red beds, with thicknesses varying from 0.5 mm up to a few centimetres. The average mineralogical composition (based on three samples) is 83% gibbsite, 11% pyrophyllite, 2–3% hematite and 2–3% anatase. Bauxites with tubular jointing (sample 15C6) show dense grey beds alternating with darker beds containing gibbsite crystals embedded in a hematite matrix. The mineralogical composition of an incompletely weathered rock (sample 15aC6) is 60% gibbsite, 10% pyrophyllite, 5% muscovite, 1% rutile, 3% hematite, 15% kaolinite and 5% quartz. In contrast, the heavily weathered rock (sample 15bC6) shows 80% gibbsite, 10% kaolinite, 5% gœthite and traces of pyrophyllite, quartz and muscovite.

Optical microscopy shows well-crystallized pyrophyllite in samples 15aC6 and 15bC6. This occurs typically in fibroradial crystal aggregates, occasionally pseudomorphed by gibbsite. Under the scanning electron microscope, these pyrophyllite aggregates are easily differentiated from muscovite (Fig. 3). Table 2 gives microprobe analysis of fresh and weathered pyrophyllites and a plot SiO_2 vs. Al_2O_3 is given in Fig. 4. Both SEM and microprobe results show a sharp contact between pyrophyllite and gibbsite.

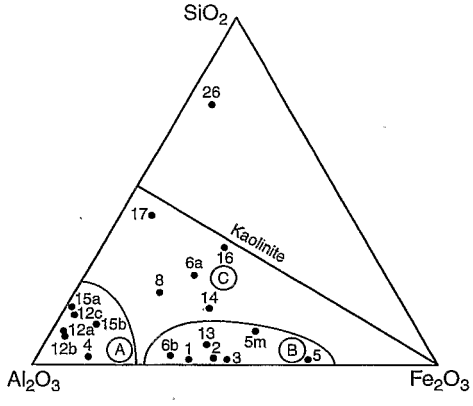

Fig. 2. SiO_2-Al_2O_3-Fe_2O_3 diagram of different facies of the Fria bauxite ore samples. *A*, bauxites; *B*, ferruginous bauxites; *C*, argillo-ferruginous bauxites, 17, weathered schist, *26*, schist

Ferruginous bauxites

These bauxites exhibit a range of facies covering porous and vesicular, platy or fragmental, and nodular and friable. They contain 38–42% Al_2O_3, 27–35% Fe_2O_3, < 5% SiO_2 and up to 3% TiO_2.

Table 2. Microprobe analyses and atomic compositions of pyrophyllite from samples 12c and 15a

	1	2	3	4	5	6	7
SiO_2	65.85	64.67	66.11	63.80	62.87	60.86	62.18
Al_2O_3	28.54	30.34	28.79	28.85	30.06	32.28	30.31
FeO	–	–	–	0.02	0.09	0.16	0.40
MgO	0.02	–	–	–	–	0.04	0.02
TiO_2	–	–	–	–	0.19	–	1.52
MnO	0.05	0.04	0.09	–	–	–	0.03
CaO	–	–	0.05	–	–	–	0.01
Na_2O	0.15	0.13	0.11	0.16	0.16	0.14	0.20
K_2O	0.06	0.06	0.07	0.02	0.12	–	–
Total	94.67	95.24	95.22	92.85	93.49	93.48	94.67
Atomic proportions on the basis of 11 oxygen atoms							
Si	3.97	3.88	3.97	3.93	3.85	3.74	3.78
Al	0.03	0.12	0.03	0.07	0.15	0.26	0.22
Al	2.00	2.03	2.00	2.02	2.02	2.07	1.96
Fe^{2+}	–	–	–	–	–	0.01	0.02
Ti	–	–	–	–	0.01	–	0.07
Na	0.02	0.02	0.01	0.02	0.02	0.02	0.02
K	–	–	0.01	–	0.01	–	–

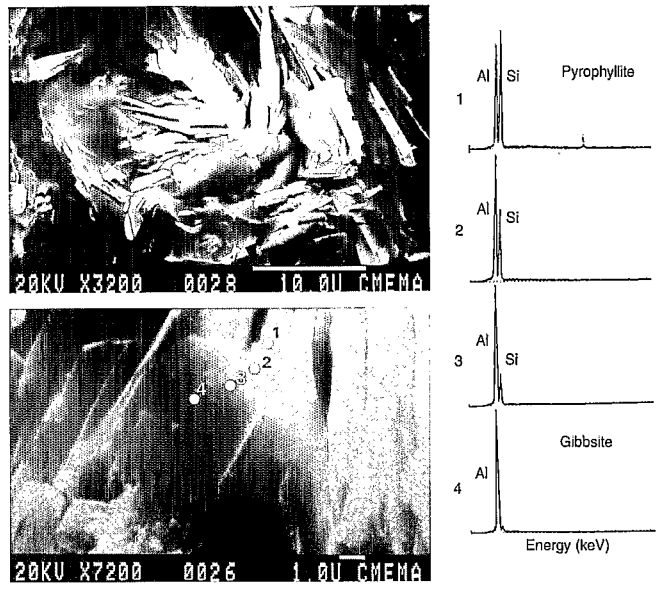

Fig. 3. Sample 15C6. Fibroradial crystalline nodule of pyrophyllite (*upper*), and pyrophyllite-gibbsite transition (*lower*) with EDS analysis points

The porous and vesicular facies (sample 1C14) is the most abundant. In this facies the texture of the parent rock has disappeared; porosity is uniformly distributed, mainly small pores <1 mm in diameter with some vesicles >1 cm. Colours range from reddish- to yellowish-brown. This facies is hard and exhibits blocky fracture on a decimetre scale, individual blocks showing associations of dark ferruginous and pale gibbsitic zones. Dark areas are formed of irregular, sub-millimetre gibbsite crystals, showing voids of dissolution, embedded in a porous hematitic matrix, indicating that the gibbsite dissolution is contemporaneous with iron accumulation. Boundaries between iron-rich dark zones and the light zones are marked by micro-nodules of hematite and small gibbsite crystals released after iron removal. Light areas are mainly composed of cryptocrystalline gibbsite. Late, well-crystallized gibbsite cutans cut former structures and correspond to the last phase of mineral formation. The overall mineral composition of the sample, based on XRD analysis, is 53% gibbsite, 15% hematite (concentrated in dark zones), 22% Al-gœthite, 3.5% anatase and 2% kaolinite. The gœthite contains 21% Al-for-Fe mole substitution, and accounts for 7% of the total Al_2O_3 content of this facies.

The platy facies (sample 2C14) exhibits alternations of white (0.5 mm) and red (1–10 mm) beds. The red beds contain hematite and have a porous and vesicular matrix, whereas the white beds are composed mainly of gibbsite crystals. This bedding appears to have been inherited from the parent schistose rock. The mineralogical composition of sample 2C14 is 60% gibbsite, 30% hematite, 2.5% gœthite, 3% anatase and 3% kaolinite.

The friable reddish-brown facies shows features of both the overlying bauxite and the underlying weathered rock (samples 3C14 and 13C6). It splits easily into centimetre-size fragments, which consist of white aluminous and dark ferruginous areas. White areas contain microcrystalline gibbsite (<300 mm) and quartz (<200 mm, 5% of sample 13C6). These fragmented quartz crystals display uniform extinction angles, this feature indicating dissolution without dislocation of the parent rock. Dark areas contain microcrystalline gibbsite disseminated in a red hematite matrix. These areas are separated by circulation zones filled with yellowish-brown cutanic deposits containing gibbsite and gœthite in equal amounts. The overall mineralogical composition of this facies is 50% gibbsite, 20% hematite, 20% gœthite, 5–10% kaolinite and 2–3% anatase. The gœthite shows the highest level of Al-for-Fe substitution of all facies of 23 mol%, containing 9% of the total Al_2O_3 content.

A fragmented ferruginous crust (53% Fe_2O_3, 25% Al_2O_3) occurs at the bottom of the profile (sample 5C14). Fragments up to 5 cm across show ferruginous areas with numerous alveolar voids, sometimes filled with quartz relicts and/or gibbsite. Ferruginous nodules (5C14) contain 38% gibbsite, 50% gœthite, 10% hematite and small

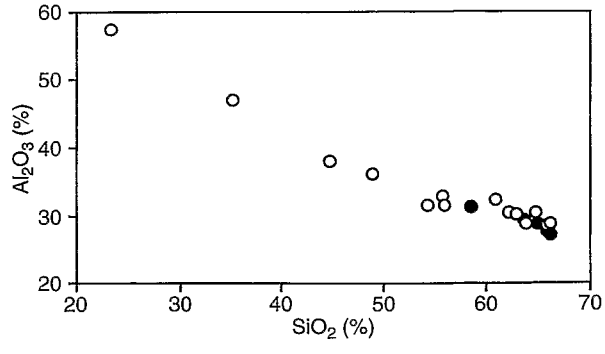

Fig. 4. Microprobe analyses of pyrophyllite. SiO_2 vs. Al_2O_3 diagram. Referenced pyrophyllite (Deer et al. 1962) (black) and fresh and weathered pyrophyllite from Fria (white)

amounts of quartz and kaolinite. The matrix (5mC14) is less ferruginous with 40% gibbsite, 20% gœthite, 22% hematite and 14% kaolinite.

Argillo-ferruginous bauxites

Examples of this facies are found at the bottom of profiles, underlying bauxites and ferruginous bauxites, where transition is progressive but irregular, and thus difficult to map. The transition zone is composed of a friable reddish-brown clay matrix (samples 6aC14 and 14C6) within which bauxite nodules (sample 6bC14) occur. At the bottom of this transition zone (sample 16C6), numbers and sizes of nodules decrease and the matrix predominates, forming the lower clay layer. Bauxite nodules (40–46% Al_2O_3) are of centimetre size, heterogeneous and generally ferruginous (23–29% Fe_2O_3). They are composed of reddish-brown to pink gibbsite embedded in a hematitic matrix. The gibbsite crystals are irregular shapes and show evidence of dissolution. Locally, vermicular kaolinite crystals occur between gibbsite remnants (Fig. 5), indicating later crystallization, probably by re-silication. Areas enriched in kaolinite are also enriched in gœthite, suggesting that iron weathering was contemporaneous with resilication. This gœthite shows high Al-substitution. The average composition of these bauxites is 20% gibbsite, 38% kaolinite, 20% gœthite, 10% hematite, 10% quartz and 2–3% anatase.

Weathered schists

The weathered schists are bluish-grey in colour and show alternating millimetre-scale, grey and white beds (samples 17C6 and 8C2). Grey beds are micaceous and ferruginous, white beds are composed of gibbsite associated with kaolinite and small muscovite crystals. Kaolinite clearly formed from muscovite but it is not clear whether gibbsite formed from kaolinite or as a result of migration of alumina from overlying beds.

Rare earth elements (REE)

REE data for the different facies are given in Fig. 6. Weathered schists (8 and 17, Fig. 6A) are depleted in REE compared to fresh rock (26). This could have been caused either by heterogeneity of the original schists or by REE leaching with fractionation between light (Ce, Nd, Sm) and heavy (Yb, Lu) rare earths. Light elements are more mobile except for Eu with shows a positive anomaly. Eu, ionized as Eu^{2+}, is less mobile (Brookins, 1984).

Argillo-ferruginous bauxites (Fig. 6B) show two kinds of distribution intermediate between weathered rocks and bauxites. This confirms the transition nature of these facies in which neoformed kaolinite after gibbsite can be observed.

Ferruginous bauxites (1,2,3 and 5, Fig. 6C) have similar REE distribution patterns, with depleted light elements. Surprisingly, the most aluminous of these samples (6b and 4) show less REE leaching.

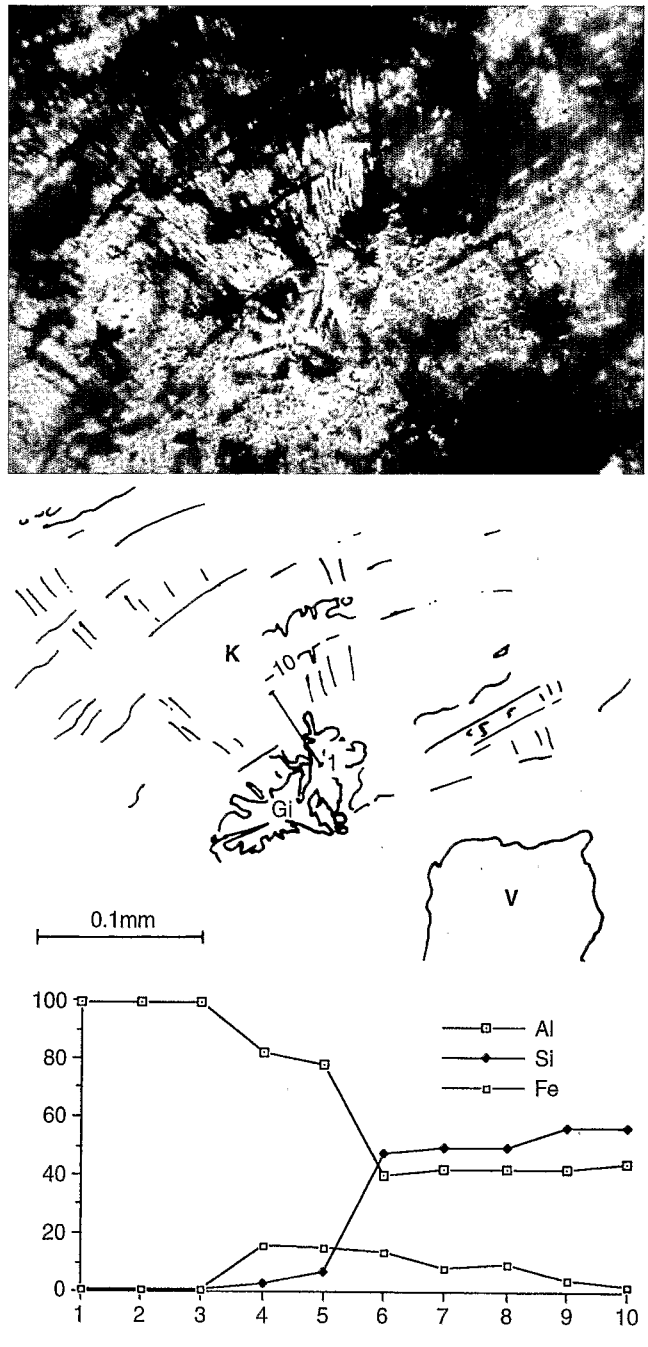

Fig. 5. Argillo-ferruginous bauxites (14C6). The crystal of gibbsite shows dissolution features. The EDS analyses (*1* to *10*) across the gibbsite-kaolinite transition. *K.* kaolinite, *Gi.* gibbsite, *V.* void

Pyrophyllite bauxites (Fig. 6D) show that the less weathered samples, which are richer in pyrophyllite (12c, 15a), are richer in REE. Weathering also shows REE fractionation and relative depletion of light REE. Heavily weathered facies (12b, 15b) have REE contents lower than ferruginous bauxites. Although the REE data set is too small for definitive conclusions, the observed variations are in agreement with petrographical observations.

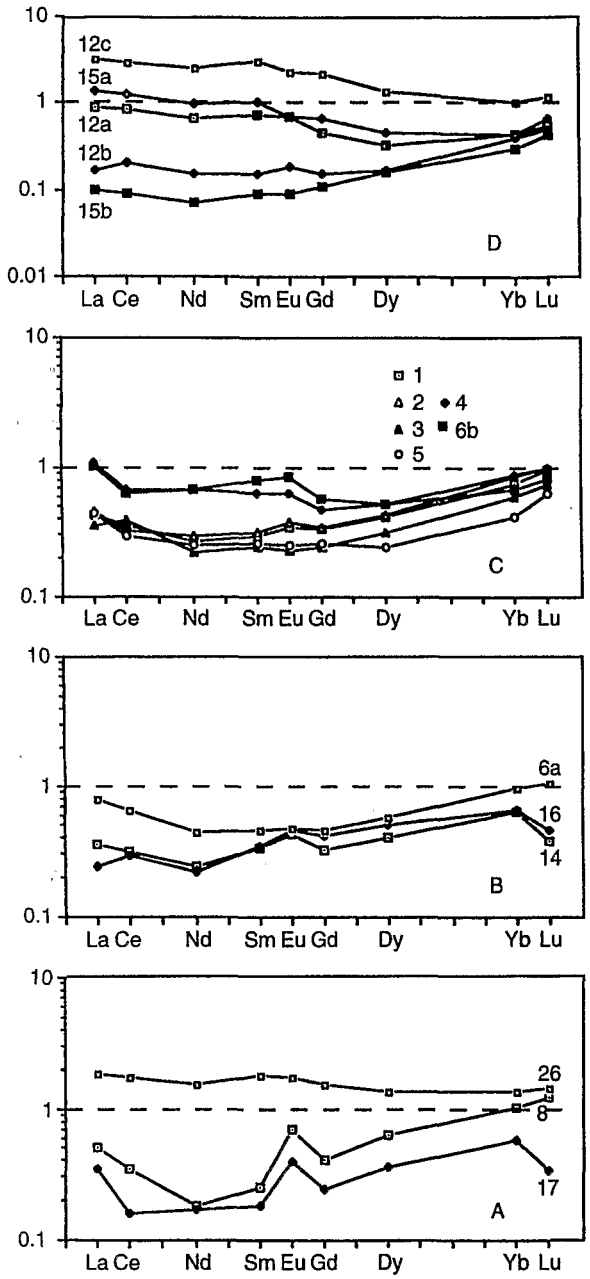

Fig. 6A–D. REE distribution patterns normalized to North American Shale Composite (Gromet et al. 1984). *Numbers* refer to samples: **A** fresh schist (*26*) and weathered schist (*8* and *17*); **B** argillo-ferruginous bauxites (*6a,16,14*); **C** bauxite (*4*) and ferruginous bauxites (*1,2,3,5* and *6b*); **D** pyrophyllite bauxite (*12* and *15*)

Mineral assemblages

Pyrophyllite-Gibbsite

Pyrophyllite, $Al_2Si_4O_{10}(OH)_2$, is a phyllosilicate containing 28–35% Al_2O_3, 64–66% SiO_2 and 5% H_2O (Deer et al., 1962). It can also contain traces (<1%) of Fe, Mg, Ca, Na and K. It forms most commonly by the action of acid hydrothermal solutions (~400 °C) on alumina-rich rocks. Dolerite sills and dykes are found in the Fria region (Bardossy and Aleva 1990) and the associated hydrothermal activity (Caïa et al. 1967) could have been responsible for transforming the schists into the pyrophyllite parent rocks of the bauxites. Muscovite is found in fresh parent rocks (sample 15aC16 contains weathered crystals), and this mineral is considered the source mineral for pyrophyllite.

Pyrophyllite is well known to be resistant to low temperature weathering (Dunoyer de Segonzac and Chamley 1968). Optical microscopy of the pyrophyllite-rich bauxite facies shows that the transformation pyrophyllite–gibbsite is pseudomorphous. REE contents decrease with increased weathering. It is very unlikely that gibbsite formed prior to pyrophyllite as if this were the case then the bauxite would contain higher-temperature Al-minerals such as diaspore. The pronounced laminar texture of the schists coupled with the resistance to weathering of the pyrophyllite could explain textural differences between porous vesicular and platy pyrophyllitic-bauxites observed in profile C6.

Gibbsite-hematite-gœthite

This assemblage is found in bauxites and ferruginous bauxites within the upper parts of the lateritic cover. These bauxites formed from schists, and the parent-rock texture is preserved within platy bauxite fragments. Intense ferruginization and removal of alumina induce formation of porous and vesicular facies, this being common in surficial samples. Lower down, alumina accumulates. Such differences are mirrored by differences in TiO_2 contents. The surficial iron-rich-bauxites (samples 1,2,3C14) have the highest TiO_2 contents (Table 1). In lateritic environments, TiO_2 is fixed in secondary anatase and usually does not migrate in profiles (Boulangé et al. 1990), and increase in TiO_2 content is thus correlated with volume decrease (linked to the change from platy to porous structure in the present samples). However, samples 5C14 and 5mC14 are iron-rich but relatively depleted in TiO_2 as a result of iron accumulation in a transition zone between bauxite and alterite. Two samples with high alumina content (4C14 and 12cC6), also have relatively high TiO_2 levels, probably due to parent rock heterogeneity.

Gibbsite-kaolinite-hematite-gœthite

This assemblage is found in argillo-ferruginous bauxites located at the bottom of the profiles. Kaolinite formed by re-silication of overlying bauxitic beds. The transition zone between this facies and overlying bauxite is very diffuse.

Implications of mineralogical composition to alumina recovery

The Bayer process used at the Friguia plant to treat bauxites from the Fria-Kimbo district employs a caustic

soda leach at 107 °C and at atmospheric pressure. This is not very aggressive compared to pressure digestion processes commonly used elsewhere.

Minerals in the Fria bauxites that remain insoluble during this atmospheric leaching process are gœthite, hematite, muscovite and pyrophyllite. Muscovite and pyrophyllite both contain structural aluminium. In samples 12C6 and 15C6 between 10–15% pyrophyllite is present and thus, 4–7% of total Al_2O_3 content of the rock would not be recovered. Gœthite also contains structural aluminium. As discussed earlier, iron mobilization at the surface (sample 1C14), but mainly at the bottom of profiles (samples 3C14 and 13C6), induces aluminous gœthite precipitation. Substitution levels are high (21–23 mole%), rendering up to 9% of the Al_2O_3 content of the rock unavailable.

However, the impact of these insoluble minerals can be minimized by combining ores with different facies. The insoluble phases are eliminated in the red mud tailings, and do not interfere with the process, unless very fine (< 10 mm). The main influence of these minerals is on the decreased alumina recovery.

Phase soluble in the Bayer process are gibbsite and clay minerals. Kaolinite is present in significant amounts in argillo-ferruginous bauxite facies (samples 6aC14, 16C6, 8C2 and 14C2). Silica extracted from kaolinite during the Bayer process precipitates as sodium alumino-silicates. Thus a portion of the dissolved aluminium is incorporated in insoluble secondary phases, reducing the efficiency of the process. Kaolinite dissolution is a function of soluble silica content of the ore and of the size and crystallinity of the kaolinite (Bardossy and Aleva 1990). Sodium alumino-silicate precipitation rates are a function of temperature and silica supersaturation. At a given temperature, precipitation of sodium alumino-silicates is thus controlled by the soluble silica level in the solution. At high dissolved silica concentrations, precipitation will be rapid, and sodium alumino-silicates will precipitate with red muds and thus easily eliminated. Conversely, if the silica level of the Bayer liquor is low ($SiO_2/Na_2O = 0.8$–0.9%), precipitation will be slower and scaling will occur along solution streams, often in heat exchangers with the gibbsite product. Scale formation on heat exchangers involves direct costs through increased energy consumption as well as indirect costs linked to maintenance. Additionally, co-precipitation of alumino-silicate with processed gibbsite decreases product quality. In such cases, minor addition of kaolinite prior to digestion of the ore can enhance silica precipitation, allowing removal in the red mud.

Efficient use of the Bayer process requires careful control of ore quality. This is an acute problem with the Fria bauxites because the transition between bauxite and altered rock is diffuse, being composed of an argillo-ferruginous facies containing neoformed kaolinite after gibbsite. Thus a detailed knowledge of the distribution of the different facies and their mineralogical compositions is necessary for planning ore extraction.

Acknowledgements. This work was supported by research grants from Aluminium Pechiney. Discussions with F. Colin proved helpful, E. Brown assisted us with the translation of this paper and R. Dassulle in drafting. Dr. D.J. Morgan made also important suggestions for improving the last draft of this paper.

References

Bardossy, G., Aleva, J.J. (1990) Lateritic bauxites. Elsevier, Amsterdam

Bessolles, B. (1977) Géologie de l'Afrique. Le craton ouest africain. BRGM

Boulangé, B., Millot, G. (1988) La distribution des bauxites sur le craton ouest-africain. Sci. Géol. 41:113–123

Boulangé, B., Carvalho, A., Melfi, A. (1990) Geochemical characteristics of African and Brazilian bauxite deposits: SiO_2-Al_2O_3-Fe_2O_3 system and Ti, Cr, V and Fe_2O_3 relations. Chem. Geol. 84:30–33

Brookins, D.G. (1984) Aqueous geochemistry of rare earth elements. In: B.R. Lipin, G.A. McKay (eds.) Geochemistry and mineralogy of rare earth elements, vol 21, pp. 201–225. Mineralogical Society of America

Caïa, J., Dietrich, J.E., Mazeas, J.P., Nataf, M. (1967) Les roches à pyrophyllite du Maroc et leurs possibilités d'utilisation dans l'industrie. Mines Géol. 26:35–50

Deer, W.A., Howia, R.A., Zussman, J. (1962) Sheet Silicates. In: Longman Scientific and Technical (eds.) Rock forming minerals, vol 3, pp. 115–120.

Dunoyer de Segonzac, G., Chamley, H. (1968) Sur le rôle joué par la pyrophyllite comme marqueur dans le cycle sédimentaire. C.R. Acad. Sci. 267:247–277

Gromet, L.P., Dymek, R.F., Haskin, L.A., Korotev, R.L. (1984) The "North American shale composite": its compilation, major and trace element characteristics. Geochim. Cosmochim. Acta. 48: 2469–2482

Mondielli, P. (1991) Etude pétrologique, minéralogique et géochimique de bauxites de Fria (Guinée). DEA. Univ. Aix-Marseille III, Marseille, France

Villeneuve, M. (1984) La suture panafricaine et l'évolution des bassins sédimentaires protérozoïques et paléozoïques de la marge NW du continent du Gondwana. Doctorat d'Etat Dissertation, Univ. Aix-Marseille III, Marseille, France

Editorial handling: D.J. Morgan